

Deterministic Control of Metamagnetic Transition of Antiferromagnetic Mott Insulator Sr_2IrO_4 by in-situ Anisotropic Strain

H. Zhang¹, L. Hao¹, J. Yang¹, J. Mutch², Z. Liu², Q. Huang¹, K. Noordhoek¹, A. F. May³, J.-H. Chu², J. W. Kim⁴, P. J. Ryan^{4,5}, H. D. Zhou¹ and Jian Liu^{1*}

¹Department of Physics and Astronomy, University of Tennessee, Knoxville, TN, USA, 37996

²Department of Physics, University of Washington, Seattle, WA, USA, 98195

³Materials Science and Technology Division, Oak Ridge National Laboratory, Oak Ridge, TN, USA, 37831

⁴Advanced Photon Source, Argonne National Laboratory, Argonne, IL, USA, 60439

⁵School of Physical Sciences, Dublin City University, Dublin 11, Ireland

Abstract

Metamagnetism in antiferromagnets exhibits distinct critical behaviors and dynamics when invoking spin reversal and rotation. Here we show a 0.05% anisotropic strain suffices to in-situ modulate the metamagnetic critical field of the Mott insulator Sr_2IrO_4 by over 50%, enabling electrical switching of the transition. Resonant x-ray scattering and model simulation reveal that the transition is completely tuned from the spin-flop to spin-flip type as the strain introduces C_4 -symmetry-breaking magnetic anisotropy. Simultaneous transport study indicates the metamagnetic responses are reflected in the large elasto- and magnetoconductance, highlighting the active charge degree of freedom in the spin-orbit-coupled Mott state and its potential for spin-electronics.

*corresponding author

Metamagnetic materials characterized by significant changes of magnetization under magnetic field is an important gateway for fundamental studies of phase transition and criticality with significant potentials for applications¹. The underlying competition between the Zeeman energy and the magnetic exchange interaction for the spin sublattice orientation provides a unique route to stabilize novel spin textures, such as spiral and helical magnetic structures². It could also enable control of the antiferromagnetic (AF) order and spin dynamics for the emerging field of AF spintronics³⁻⁶. However, controlling metamagnetic transition has yet been challenging. Varying magnetic field and temperature are the two most common methods but not ideal for applications⁷. Fundamentally, metamagnetism critically depends on spin anisotropy, which determine whether the moments response to the magnetic field by spin reversal or rotation. This generally categorizes the metamagnetic transition of antiferromagnets into the spin-flip and spin-flop types for systems. The former involves a sudden flip of half of the AF spins when the magnetic field is parallel to the easy axis, whereas the latter undergoes spin rotation first to the hard axis and then gradually towards the field. In addition, when the field is perpendicular to the easy axis, metamagnetic transition will become a continuous type of spin rotation. The spin-flip transition is thus often first order, whereas the gradual spin rotation of the spin-flop and continuous types are second order. Anisotropy can thus afford an effective knob for tuning metamagnetism, but it is also difficult to control to substantial extension since its energy scale largely determined by spin-orbit-coupling (SOC) strength and lattice symmetry.

Sr_2IrO_4 is a representative iridate compound with an interesting quasi-two-dimensional pseudospin-half AF Mott insulating state⁸⁻¹⁹. In particular, by stabilizing the pseudospin-half state, the strong SOC of Ir plays a profound yet often hidden role in the low-energy physics, such as the large anisotropic exchanges that are symmetry-invariant and have no contribution to the magnetic

anisotropy^{11, 20-22}. Indeed, Sr_2IrO_4 exhibits incredible phenomenological analogy to the weakly spin-orbit-coupled high- T_c cuprates²³⁻³³. Figure 1a shows the tetragonal crystal structure of Sr_2IrO_4 and its magnetic structures below $T_N \sim 230\text{K}$ ^{8, 10}. The key role of SOC is to introduce canting of the in-plane AF moments. The canted moments of different Ir planes cancel each other out by stacking in a $\uparrow\text{-}\uparrow\text{-}\downarrow\text{-}\downarrow$ sequence at zero field and are aligned through a metamagnetic transition triggered by an in-plane magnetic field H . Interestingly, this metamagnetic transition is accompanied with a giant magnetoconductance (MC)³⁴⁻³⁹, indicating a strong charge response to the spin degree of freedom, which would be absent in a purely Mott-character insulator behavior.

Here we show that an anisotropic strain less than 0.1%, achieved through a piezo device, is sufficient to in-situ tune the metamagnetic transition among all the three regimes (spin-flop, spin-flip and continuous) in Sr_2IrO_4 by controlling the C_4 -symmetry-breaking anisotropy. Our results show that the unique combination of strong SOC and weak incipient magnetic anisotropy⁴⁰⁻⁴³ lead to a remarkably efficient spin-lattice coupling that enables metamagnetic switching of not only the pseudospin ordering but also the electronic conductance in such a novel Mott state. The emergence of the spin-lattice coupling under the C_4 -symmetry-breaking field is consistent with the recently proposed pseudo-Jahn-Teller effect of spin-orbit-entangled correlated electrons^{44, 45}.

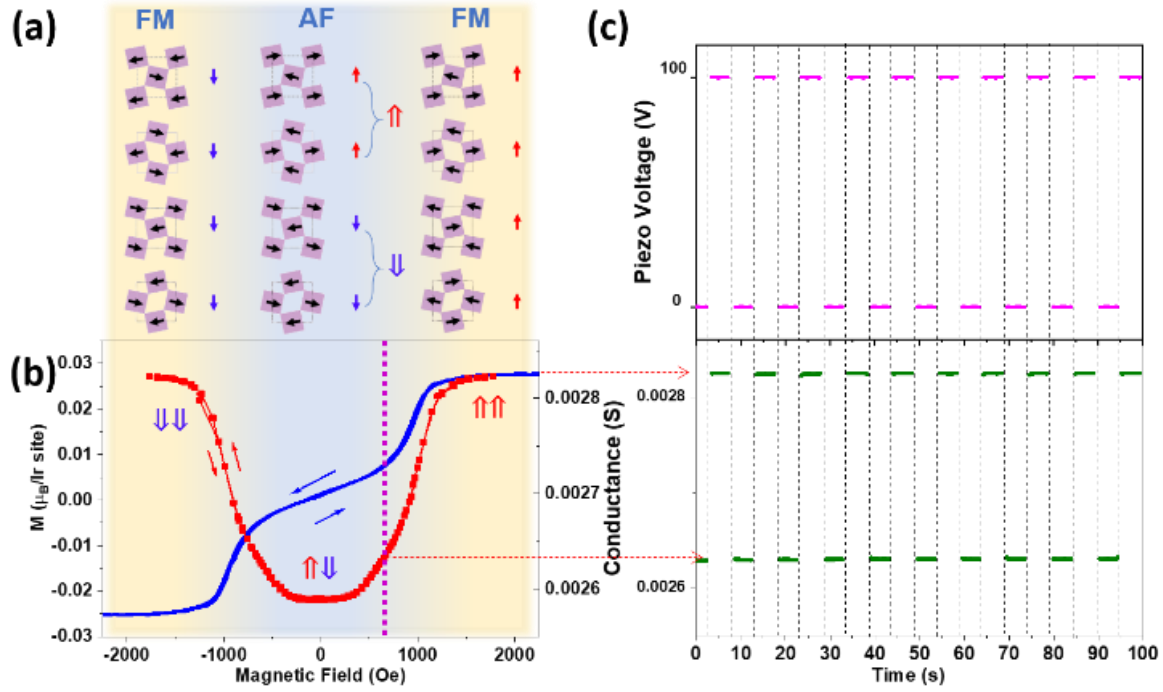


Figure 1 Electrical metamagnetic switching of Sr_2IrO_4 (a) Pseudospin configuration of the AFM state (middle) and the corresponding FM structure under positive (right) and negative (left) magnetic field along b -axis. The pseudospins are canted by $\sim 12^\circ$, owing to the strong SOC and octahedral rotation^{13, 14, 46-49}. It should be noted that, strictly speaking, both states are canted AF orders of the pseudospins. (b) Magnetoconductance (MC) curve of freestanding Sr_2IrO_4 single crystal (red) and the magnetic susceptibility (blue) at 210K. (c) Switching of the MC at 600Oe by tuning the in-situ anisotropic strain along the a -axis (i.e., $\epsilon//a$) while fixing $H//b$ near the transition.

Sr_2IrO_4 single crystal were grown using a SrCl_2 flux in Pt crucibles. Details of the growth procedure can be found in ref^{50, 51}. The magnetization curve at 210K indicates the metamagnetic transition takes place at ~ 1000 Oe, where a significant increase is also seen in the MC curve, consistent with previous reports. For instance, a positive MC of $\sim 10\%$ is observed within ± 250 Oe of the transition region. One may consider this MC as a spin-valve-like⁵² behavior at the atomic scale, where the neighboring Ir planes with parallel canted moments pair up as one ferromagnetic (FM) slab ($\uparrow\text{-}\uparrow \rightarrow \uparrow\uparrow$), and the parallel ($\uparrow\uparrow$) and antiparallel ($\uparrow\downarrow$) configurations of the adjacent

FM slabs create two conductive values as the “on” and “off” states. For simplicity, the two configurations are respectively denoted by FM and AF states hereafter. To introduce a symmetry-breaking anisotropic strain ε within the Ir plane, we mounted the sample onto a piezo actuator⁵³ with maximum deliverable strain $\sim 0.1\%$. Surprisingly, despite such small strain strength, we found a robust and almost complete on-and-off switch of the conductance with $H//b$ at 600 Oe (Fig. 1c) when alternating the piezo voltage between +100 and 0 V to stretch the sample along a -axis at 210 K. We further measured the actual strain induced in the sample with synchrotron x-ray diffraction (see supplement) and found the anisotropic strain to be $\sim 0.05\%$ at 100 V. This elastoconductance (EC) response indicates a highly efficient anisotropic strain-control of the metamagnetic transition by breaking the tetragonality of the layered structure.

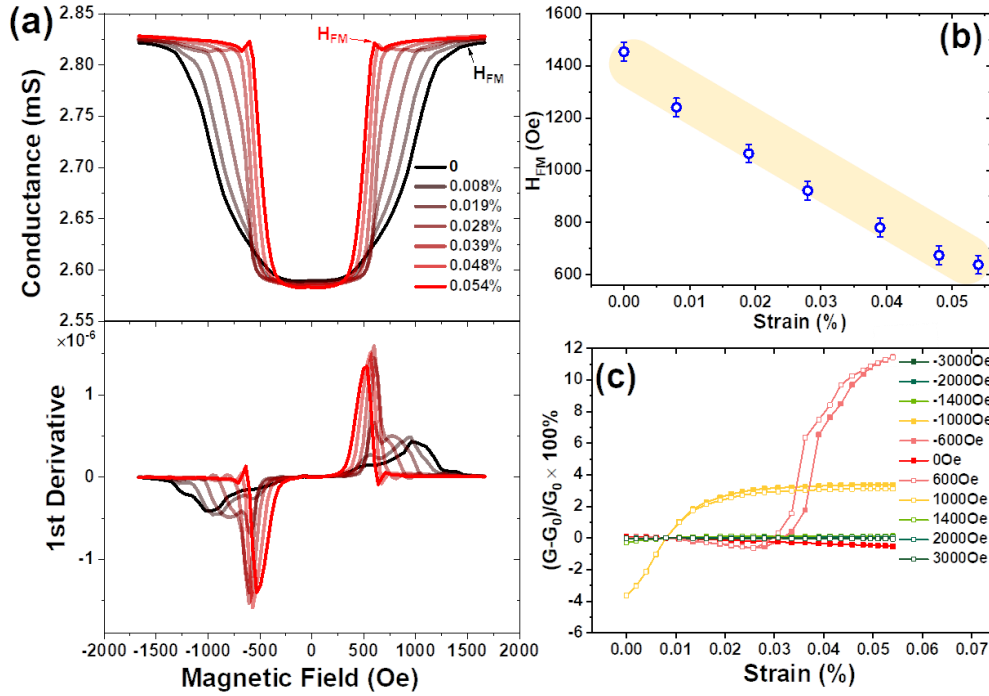


Figure 2 Magnetoconductance under anisotropic strain (a) Magnetoconductance (top) and its 1st derivative (bottom) under different value of anisotropic strain. (b) shift of the field H_{FM} with strain where the metamagnetic transition is completed. (c) Relative change in resistance respect to the zero-strained state under different magnetic and strain field.

To shed light onto this strain effect, we performed a systematic MC study (Fig. 2a) at various strain values under the same geometry. A clear shift of the metamagnetic transition by hundreds of Oersteds can be immediately noticed. Figure 2b shows that the magnetic field H_{FM} , where the transition fully enters the FM state, displays a large systematic decrease from 1500 to 600 Oe within the $\sim 0.05\%$ range of strain. Figure 2c shows a complementary result of EC by fixing H and continuously modulating ε via the voltage-control. The EC response is weak and linear at both large and small magnetic fields, but exhibits a highly nonlinear and asymmetrical behavior when H is near the transition region. In particular, the EC at 600 Oe reaches $\sim 10\%$, almost matching the full conductance modulation across the transition (Fig. 1c). The nonlinearity and

asymmetry of the strain response is also manifested in the MC curves (Fig. 2a top) as the transition region evolves from a gradual modulation at small strains to an abrupt jump at higher strains. This behavior is more evident in the derivative curves (Fig. 2a bottom), which show that the downshifting of the transition corresponds to the downshifting of the primary broad peak with the emergence of a second peak at lower fields, indicative of a two-step transition. As strain increases, the secondary peak grows, sharpens, and eventually becomes the primary peak with the original broad primary peak merging in and finally disappearing.

The complex responses of the metamagnetic transition indicates a nontrivial mechanism underlying the highly efficient strain-control. To gain microscopic insights, we performed x-ray resonant magnetic scattering (XRMS) at the Ir L_3 -edge under both strain and magnetic fields with *in-situ* conductance measurement (Fig. 3a). At 210 K, we observed the magnetic peaks corresponding to the two 90° AF domains at zero field with the canted moments along the a -axis (AF_a) and b -axis (AF_b), respectively. When applying $H//b$ (Fig. 3c), the AF_b domain are first gradually converted into the AF_a domain. The magnetic peak of the FM state already emerges before this detwinning process is finished, but increases significantly only when the AF_a peak intensity begins to decrease until the completion of the metamagnetic transition. This magnetic detwinning process is consistent with the previous report⁴⁵ but also displays a strong strain dependence. Interestingly, when increasing ε , both the AF_b-to-AF_a and AF_a-to-FM processes are clearly sharpened, while being pushed toward higher and lower fields, respectively (Fig. 3d&e). The overall result is that the stable region of the AF_a domains is strongly reduced and eventually diminished, driving the system into a new regime where the transition directly occurs between the AF_b and FM state through a sharp jump (Fig. 3f). In other words, the applied anisotropic strain detwins the AF domains but in a competing fashion against the magnetic field, which in turn

stabilizes the FM state at smaller H . The evolution from the AF_b -to- AF_a -to-FM process to the AF_b -to-FM process is well consistent with the two-step-to-one-step behavior of the transition from the MC analysis (Fig. 2b). Indeed, MC (Fig. 3c-f) is found to always closely follow the modulation of the FM peak under anisotropic strain.

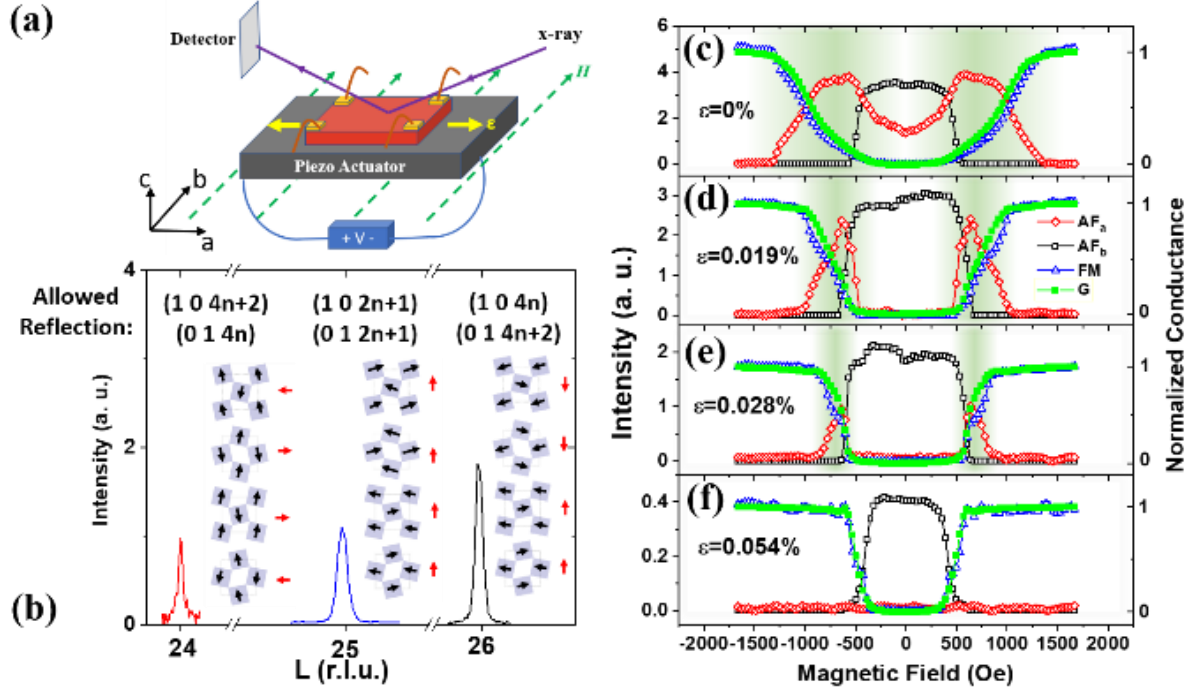


Figure 3 Resonant magnetic x-ray scattering with in-situ transportation measurement (a) Schematic setup of the measurement. (b) The AF_a (left), AF_b (right) and FM (middle) structures and the allowed reflection (0 1 L)-scans of the magnetic peaks at 210K. (c-f) Magnetic reflections between -2000Oe and 2000Oe taken at 210K with 0% to 0.054% tensile strain along a-axis. Red diamonds are the (0 1 24) reflection associated with AF_a , black squares are the (0 1 22) reflection from AF_b , the blue triangles are the FM peak (0 1 25), and the green curve is the in-situ conductance measurement.

Given that the conductance is a good measure of the FM order, we constructed a ε - H phase diagram based on the MC and EC in Fig. 2 and designated the AF domains based on XRMS. The

phase diagram shown in Fig. 4a clearly illustrates that the broad transition region corresponds to the gradual AF_a-to-FM processes, which is suppressed by increasing ε and eventually removed at $\varepsilon > 0.03\%$, giving rise to the downshifting and sharpening of the transition toward the AF_b-to-FM jump. These different magnetic structure evolutions represent different types of the metamagnetic transition, which can be well captured in a picture where the applied strain efficiently modulates the uniaxial anisotropy. The AF_b-to-FM jump is essentially a spin-flip transition, which occurs when the magnetic field is along the easy axis of an antiferromagnet, i.e., the b -axis in this case. Due to the strong uniaxial pseudospin anisotropy, the only choice of the system is to flip half of the spins when the Zeeman energy gain is bigger than the inter-slab magnetic exchange energy lost. On the other hand, when the uniaxial anisotropy is weak, the system may first rotate all the spins by 90° to enable canting and accommodate the Zeeman energy gain in the expense of the anisotropy energy. The canting angle continuously increases with the magnetic field until all the AF exchange energy is lost. This is the spin-flop-type metamagnetic transition, corresponding to the AF_b-to-AF_a-to-FM process. The observed gradual increase of the FM peak intensity at the expense of the AF_a peak essentially reflects the change of the angle between the two slabs.

To be quantitative, we simulated the ground state phase diagram with a minimum model of a two-slab cell, where the free energy can be written as:

$$F(\alpha_1, \alpha_2) = J_c \cos(\alpha_1 - \alpha_2) - h \cos(\alpha_1) - h \cos(\alpha_2) - K_u (\cos^2 \alpha_1 + \cos^2 \alpha_2) - K_b [\cos(2\alpha_1) + \cos(2\alpha_2)]^2$$

where J_c represents the inter-slab exchange energy; α_1 and α_2 are the angles of the slab magnetization \mathbf{m} with respect to $H//b$ -axis; $h = mH$ is the Zeeman energy. K_u and K_b represent the strain-induced uniaxial anisotropy and the bi-axial anisotropy due to C_4 symmetry, respectively. The simulated $K_u - h$ phase diagram in the unit of J_c is shown in Fig. 4b, and reproduces the

overall experimental results very well with spin-flip and spin-flop phase boundaries. The relative angle between the two slabs is indeed continuously modulated within the AF_a state. This model further predicts that a broad continuous transition would occur at large but negative K_u , which corresponds to an easy a -axis under a large negative ε . While negative ε is unreachable due to the voltage limit of the piezo actuator, we realize this scenario by simply applying $H \perp b$. We indeed observed from MC a significant broadening of the metamagnetic transition into an extended gradual process with H_{FM} increased to ~ 2300 Oe (Fig. 4c), which is four times of the $H_{\text{FM}} \sim 600$ Oe with $H // b$.

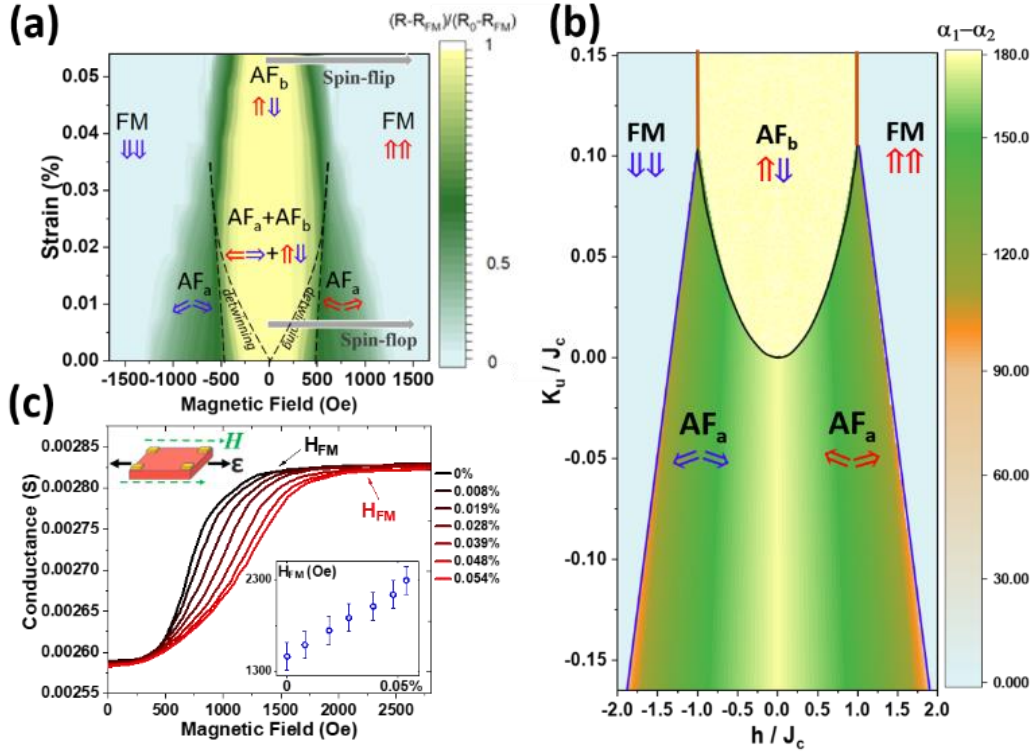


Figure 4 Strain-magnetic field phase diagram of Sr_2IrO_4 (a) Experimental and (b) calculated (with $K_b=0.06J_c$) Phase diagram of the Sr_2IrO_4 at 210K with varies anisotropic strain and magnetic field values. With negative strain value $H//b$ would be along the hard axis and the metamagnetic transition would be dramatically broadened. The simulated result in the spin flip regime (straight line) is a robust behavior regardless the value used for K_b . Details of the model can be found in the supplementary. (c) Measured MC curves (solid lines) with both magnetic field and anisotropic strain along a-axis. The inset shows the extract point H_{FM} where the metamagnetic transition is completed with different strain values.

The ability of tuning the metamagnetic transition into all three regimes with $\varepsilon < 0.1\%$ demonstrates the high sensitivity of the pseudospin-half state to lattice modulation. One can see that K_u is only $\sim 10\%$ of J_c when entering the spin-flip regime, while h/J_c is always ~ 1 near the transition. We estimated $J_c \sim 313 \text{ neV}$ at 210 K (supplementary), rendering a small $K_u \sim 31 \text{ neV}$ for full control of the transition under $\varepsilon \sim 0.5\%$. Given the fact that the transition occurs microscopically

through the flip/flop of the staggered moment, the magnetoelastic coupling coefficient is extracted to be $\sim 0.5 \text{ meV}/\mu_B^2$ at 210 K. Its microscopic mechanism can be attributed to the recently proposed pseudo-Jahn-Teller effect, which is an extension of Jahn-Teller effect to spin-entangled orbital singlet^{44, 54}. It was suggested that the AF order of Sr_2IrO_4 is accompanied with a ferro-pseudospin quadrupolar order that originates from mixing of pseudospin ground and excited states, and spontaneously breaks the C_4 symmetry of the lattice, stabilizing an easy axis with orthorhombic distortion at the level of 10^{-4} . The strain-induced pseudospin anisotropy here is essentially the demonstration of the inverse effect, where the AF order is controlled by continuous structural modulation of the pseudospin quadrupole. As shown, this mechanism is remarkably efficient, allowing exploitation of piezo-strain for effective electrical tuning of the spin-orbit and the metamagnetism.

It is interesting to highlight the fact that such in-situ strain-tuned metamagnetism of AF Mott insulating Sr_2IrO_4 is always accompanied with significant MC and EC responses. The charge hopping is clearly highly sensitive to the relative staggered moment orientation of adjacent layers, which is similar to La_2CuO_4 ⁵⁵. Theoretical investigations beyond the effective spin model could lead to comprehensive understanding⁵⁶. Our results demonstrated that the application of anisotropic strain is an appealing route to probe the rich physics of the spin-orbit-charge interplay. One can anticipate interesting in-situ strain control of other static and even dynamic electromagnetic responses⁵⁷⁻⁶⁰.

Acknowledgement: J.L. and H.D.Z. acknowledges support from the Organized Research Unit Program at the University of Tennessee. Sample synthesis (A.F.M.) was supported by the U. S. Department of Energy, Office of Science, Basic Energy Sciences, Materials Sciences and Engineering Division. The in-situ strain control and measurement setup is partially supported by AFOSR DURIP Award FA9550-19-1-0180; the Scholarly Activity and Research Incentive Fund (SARIF) at the University of Tennessee and as part of Programmable Quantum Materials, an Energy Frontier Research Center funded by the U.S. Department of Energy (DOE), Office of Science, Basic Energy Sciences (BES), under award DE-SC0019443. Z.L. and J.H.C. acknowledge the support of the David and Lucile Packard Foundation. Transport measurement is supported by the U. S. Department of Energy under grant No. DE-SC0020254 and the Electromagnetic Property (EMP) Lab Core Facility at the University of Tennessee. This research used resources of the Advanced Photon Source, a U.S. Department of Energy (DOE) Office of Science User Facility operated for the DOE Office of Science by Argonne National Laboratory under Contract No. DE-AC02-06CH11357. The authors thank David Mandrus, Mark P. M. Dean and Cristian Batista for valuable discussions; Randal R. McMillan and Bennett S. Waddell for providing technical support in making strain devices and sample holders.

References

1. E. Stryjewski and N. Giordano, *Adv. Phys.* **26**, 487-650 (1977).
2. D. A. Sokolov, N. Kikugawa, T. Helm, H. Borrmann, U. Burkhardt, R. Cubitt, J. S. White, E. Ressouche, M. Bleuel, K. Kummer, A. P. Mackenzie and U. K. Rößler, *Nat. Phys.* **15** (7), 671-677 (2019).
3. A. Manchon, H. C. Koo, J. Nitta, S. M. Frolov and R. A. Duine, *Nat. Mater.* **14** (9), 871-882 (2015).
4. T. Jungwirth, X. Marti, P. Wadley and J. Wunderlich, *Nat. Nanotechnol.* **11** (3), 231-241 (2016).
5. V. Baltz, A. Manchon, M. Tsoi, T. Moriyama, T. Ono and Y. Tserkovnyak, *Rev. Mod. Phys.* **90** (1), 015005 (2018).
6. L. Šmejkal, Y. Mokrousov, B. Yan and A. H. MacDonald, *Nat. Phys.* **14** (3), 242-251 (2018).
7. C. Song, Y. You, X. Chen, X. Zhou, Y. Wang and F. Pan, *Nanotechnology* **29** (11), 112001 (2018).
8. G. Cao, J. Bolivar, S. McCall and J. E. Crow, *Phys. Rev. B* **57**, R11039-R11042 (1998).
9. B. J. Kim, H. Jin, S. J. Moon, J. Y. Kim, B. G. Park, C. S. Leem, J. Yu, T. W. Noh, C. Kim, S. J. Oh, J. H. Park, V. Durairaj, G. Cao and E. Rotenberg, *Phys. Rev. Lett.* **101** (7), 076402 (2008).
10. B. J. Kim, H. Ohsumi, T. Komesu, S. Sakai, T. Morita, H. Takagi and T. Arima, *Science* **323** (5919), 1329-1332 (2009).
11. G. Jackeli and G. Khaliullin, *Phys. Rev. Lett.* **102** (1), 017205 (2009).
12. R. Schaffer, E. Kin-Ho Lee, B. J. Yang and Y. B. Kim, *Rep. Prog. Phys.* **79** (9), 094504 (2016).
13. G. Cao and P. Schlottmann, *Rep. Prog. Phys.* **81** (4), 042502 (2018).
14. J. Bertinshaw, Y. K. Kim, G. Khaliullin and B. J. Kim, *Annu. Rev. Condens. Matter Phys.* **10** (1), 315-336 (2019).
15. R. Arita, J. Kunes, A. V. Kozhevnikov, A. G. Eguiluz and M. Imada, *Phys. Rev. Lett.* **108** (8), 086403 (2012).

16. S. Boseggia, R. Springell, H. C. Walker, H. M. Ronnow, C. Ruegg, H. Okabe, M. Isobe, R. S. Perry, S. P. Collins and D. F. McMorrow, *Phys. Rev. Lett.* **110** (11), 117207 (2013).
17. T. Takayama, A. Matsumoto, G. Jackeli and H. Takagi, *Phys. Rev. B* **94** (22) (2016).
18. S. J. Moon, H. Jin, K. W. Kim, W. S. Choi, Y. S. Lee, J. Yu, G. Cao, A. Sumi, H. Funakubo, C. Bernhard and T. W. Noh, *Phys. Rev. Lett.* **101** (22), 226402 (2008).
19. D. H. Torchinsky, H. Chu, L. Zhao, N. B. Perkins, Y. Sizyuk, T. Qi, G. Cao and D. Hsieh, *Phys. Rev. Lett.* **114** (9), 096404 (2015).
20. J. G. Rau, E. K.-H. Lee and H.-Y. Kee, *Annu. Rev. Condens. Matter. Phys.* **7** (1), 195-221 (2016).
21. L. Hao, D. Meyers, H. Suwa, J. Yang, C. Frederick, T. R. Dasa, G. Fabbri, L. Horak, D. Kriegner, Y. Choi, J.-W. Kim, D. Haskel, P. J. Ryan, H. Xu, C. D. Batista, M. P. M. Dean and J. Liu, *Nat. Phys.* **14** (8), 806-810 (2018).
22. S. Calder, D. M. Pajerowski, M. B. Stone and A. F. May, *Phys. Rev. B* **98** (22), 220402 (2018).
23. H. Watanabe, T. Shirakawa and S. Yunoki, *Phys. Rev. Lett.* **105** (21), 216410 (2010).
24. F. Wang and T. Senthil, *Phys. Rev. Lett.* **106** (13), 136402 (2011).
25. J. Kim, D. Casa, M. H. Upton, T. Gog, Y. J. Kim, J. F. Mitchell, M. van Veenendaal, M. Daghofer, J. van den Brink, G. Khaliullin and B. J. Kim, *Phys. Rev. Lett.* **108** (17), 177003 (2012).
26. Y. K. Kim, Krupin, O., Kenlinger, J. D., Bostwick, A., Rotenberg, E., Zhao, Q., Mitchell, J. F., Allen, J. W., Kim, B. J. , *Science* **345** (6193), 187-190 (2014).
27. Y. K. Kim, N. H. Sung, J. D. Denlinger and B. J. Kim, *Nat. Phys.* **12** (1), 37-41 (2015).
28. Y. J. Yan, M. Q. Ren, H. C. Xu, B. P. Xie, R. Tao, H. Y. Choi, N. Lee, Y. J. Choi, T. Zhang and D. L. Feng, *Phys.Rev. X* **5** (4), 041018 (2015).
29. R. Comin, R. Sutarto, F. He, E. H. da Silva Neto, L. Chauviere, A. Frano, R. Liang, W. N. Hardy, D. A. Bonn, Y. Yoshida, H. Eisaki, A. J. Achkar, D. G. Hawthorn, B. Keimer, G. A. Sawatzky and A. Damascelli, *Nat. Mater.* **14** (8), 796-800 (2015).
30. L. Zhao, D. H. Torchinsky, H. Chu, V. Ivanov, R. Lifshitz, R. Flint, T. Qi, G. Cao and D. Hsieh, *Nat. Phys.* **12** (1), 32-36 (2015).
31. J. Jeong, Y. Sidis, A. Louat, V. Brouet and P. Bourges, *Nat. commun.* **8**, 15119 (2017).

32. X. Chen, J. L. Schmehr, Z. Islam, Z. Porter, E. Zoghlin, K. Finkelstein, J. P. C. Ruff and S. D. Wilson, *Nat. Commun.* **9** (1), 103 (2018).
33. S. Di Matteo and M. R. Norman, *Phys. Rev. B* **94** (7) (2016).
34. M. Ge, T. F. Qi, O. B. Korneta, D. E. De Long, P. Schlottmann, W. P. Crummett and G. Cao, *Phys. Rev. B* **84** (10), 100402 (2011).
35. C. Wang, H. Seinige, G. Cao, J. S. Zhou, J. B. Goodenough and M. Tsoi, *Phys. Rev. X* **4** (4), 041034 (2014).
36. I. Fina, X. Marti, D. Yi, J. Liu, J. H. Chu, C. Rayan-Serrao, S. Suresha, A. B. Shick, J. Zelezny, T. Jungwirth, J. Fontcuberta and R. Ramesh, *Nat. Commun.* **5**, 4671 (2014).
37. C. Wang, H. Seinige, G. Cao, J. S. Zhou, J. B. Goodenough and M. Tsoi, *J. Appl. Phys.* **117** (17) (2015).
38. N. Lee, E. Ko, H. Y. Choi, Y. J. Hong, M. Nauman, W. Kang, H. J. Choi, Y. J. Choi and Y. Jo, *Adv. Mater.* **30** (52), e1805564 (2018).
39. H. Wang, C. Lu, J. Chen, Y. Liu, S. L. Yuan, S.-W. Cheong, S. Dong and J.-M. Liu, *Nat. Commun.* **10** (1), 2280 (2019).
40. S. Fujiyama, H. Ohsumi, T. Komesu, J. Matsuno, B. J. Kim, M. Takata, T. Arima and H. Takagi, *Phys. Rev. Lett.* **108** (24), 247212 (2012).
41. J. G. Vale, S. Boseggia, H. C. Walker, R. Springell, Z. Feng, E. C. Hunter, R. S. Perry, D. Prabhakaran, A. T. Boothroyd, S. P. Collins, H. M. Rønnow and D. F. McMorrow, *Phys. Rev. B* **92** (2) (2015).
42. L. Fruchter, D. Colson and V. Brouet, *J. Phys. Condens. Matter.* **28** (12), 126003 (2016).
43. S. Calder, J. W. Kim, A. E. Taylor, M. H. Upton, D. Casa, G. Cao, D. Mandrus, M. D. Lumsden and A. D. Christianson, *Phys. Rev. B* **94** (22) (2016).
44. H. Liu and G. Khaliullin, *Phys. Rev. Lett.* **122** (5), 057203 (2019).
45. J. Porras, J. Bertinshaw, H. Liu, G. Khaliullin, N. H. Sung, J. W. Kim, S. Francoual, P. Steffens, G. Deng, M. M. Sala, A. Efimenko, A. Said, D. Casa, X. Huang, T. Gog, J. Kim, B. Keimer and B. J. Kim, *Phys. Rev. B* **99** (8), 085125 (2019).
46. S. Boseggia, H. C. Walker, J. Vale, R. Springell, Z. Feng, R. S. Perry, M. Moretti Sala, H. M. Ronnow, S. P. Collins and D. F. McMorrow, *J. Phys. Condens. Matter.* **25** (42), 422202 (2013).

47. F. Ye, S. Chi, B. C. Chakoumakos, J. A. Fernandez-Baca, T. Qi and G. Cao, *Phys. Rev. B* **87** (14), 140406 (2013).
48. C. Dhital, T. Hogan, Z. Yamani, C. de la Cruz, X. Chen, S. Khadka, Z. Ren and S. D. Wilson, *Phys. Rev. B* **87** (14), 144405 (2013).
49. D. H. Torchinsky, H. Chu, L. Zhao, N. B. Perkins, Y. Sizyuk, T. Qi, G. Cao and D. Hsieh, *Phys. Rev. Lett.* **114** (9), 096404 (2015).
50. N. H. Sung, H. Gretarsson, D. Proepper, J. Porras, M. Le Tacon, A. V. Boris, B. Keimer and B. J. Kim, *Philos. Mag.* **96** (4), 413-426 (2016).
51. A. F. May, H. Cao and S. Calder, *Phys. Rev. Mater.* **2** (9), 094406 (2018).
52. B. G. Park, J. Wunderlich, X. Marti, V. Holy, Y. Kurosaki, M. Yamada, H. Yamamoto, A. Nishide, J. Hayakawa, H. Takahashi, A. B. Shick and T. Jungwirth, *Nat. Mater.* **10** (5), 347-351 (2011).
53. J.-H. Chu, J. Hsueh-Hui Kuo, G. Analytis and I. R. Fisher, *Science* **337**, 710-712 (2012).
54. E. M. Plotnikova, M. Daghofer, J. van den Brink and K. Wohlfeld, *Phys. Rev. Lett.* **116** (10), 106401 (2016).
55. T. Thio, C. Y. Chen, B. S. Freer, D. R. Gabbe, H. P. Jenssen, M. A. Kastner, P. J. Picone, N. W. Preyer and R. J. Birgeneau, *Phys. Rev. B* **41** (1), 231-239 (1990).
56. I. V. Solovyev, V. V. Mazurenko and A. A. Katanin, *Phys. Rev. B* **92** (23) (2015).
57. S. Bahr, A. Alfonsov, G. Jackeli, G. Khaliullin, A. Matsumoto, T. Takayama, H. Takagi, B. Büchner and V. Kataev, *Phys. Rev. B* **89** (18), 180401 (2014).
58. Y. Gim, A. Sethi, Q. Zhao, J. F. Mitchell, G. Cao and S. L. Cooper, *Phys. Rev. B* **93** (2), 024405 (2016).
59. M. P. Dean, Y. Cao, X. Liu, S. Wall, D. Zhu, R. Mankowsky, V. Thampy, X. M. Chen, J. G. Vale, D. Casa, J. Kim, A. H. Said, P. Juhas, R. Alonso-Mori, J. M. Glownia, A. Robert, J. Robinson, M. Sikorski, S. Song, M. Kozina, H. Lemke, L. Patthey, S. Owada, T. Katayama, M. Yabashi, Y. Tanaka, T. Togashi, J. Liu, C. Rayan Serrao, B. J. Kim, L. Huber, C. L. Chang, D. F. McMorrow, M. Forst and J. P. Hill, *Nat. Mater.* **15** (6), 601-605 (2016).
60. D. Afanasiev, A. Gatilova, D. J. Groenendijk, B. A. Ivanov, M. Gibert, S. Gariglio, J. Mentink, J. Li, N. Dasari, M. Eckstein, T. Rasing, A. D. Caviglia and A. V. Kimel, *Phys. Rev. X* **9** (2) (2019).
- 61 See Supplementary Materials for experimental details.

